Regular Article

Effect of a pre-aging treatment on the mechanical behaviors of $Ni_{50.3}Ti_{49.7 - x}Hf_x$ (x ≤ 9 at.%) Shape memory alloys

Behnam Amin-Ahmadi [a,*], Thomas Gallmeyer [a], Joseph G. Pauza [a], Tom W. Duerig [b], Ronald D. Noebe [c], Aaron P. Stebner [a]

[a] Mechanical Engineering, Colorado School of Mines, Golden, CO 80401, USA
[b] Confluent Medical Technologies, Fremont, CA 94539, USA
[c] NASA Glenn Research Center, Materials and Structures Division, Cleveland, OH 44135, USA

ABSTRACT

Transmission electron microscopy and mechanical testing were used to determine the effect of pre-aging (300 °C for 12 h) on microstructure and mechanical behavior of a series of $Ni_{50.3}Ti_{49.7 - x}Hf_x$ shape memory alloys (x = 6, 8, 8.5, 9 at.%) prior to normal aging at 550 °C for 3.5 h. Pre-aging was found to promote homogenous nucleation of nanosized H-phase precipitates, resulting in improved mechanical stability and strength and 4% recoverable compression strain without permanent deformation. The absence of pre-aging generally resulted in heterogeneous formations of larger H-phase precipitates, primarily clustered along grain boundaries, and correlated with poorer mechanical behavior.

© 2017 Acta Materialia Inc. Published by Elsevier Ltd. All rights reserved.

NiTi shape memory alloys (SMAs) have been successfully used in many different fields of engineering because of their functional properties that include shape memory effect (SME) and superelasticity (SE) [1, 2]. These properties are due to the occurrence of reversible, thermoelastic martensitic transformations [1–5]. However, work hardening and subsequent aging in the range of 400–550 °C are required to obtain superelastic performances suitable for most applications [2, 5–9]. This secondary processing is required because in solid-solution-annealed NiTi, the yield stress is typically less than or equal to the operational transformation stresses. However, the aforementioned aging results in nano-precipitate strengthening via the metastable Ni_4Ti_3 phase [1–8], while cold work imparts dislocation forest structures, the combination of which increase the yield strength of the alloy well above the operational transformation stresses.

Recently, additive manufacturing of NiTi has gained significant attention, as near-net-shaping technology allows for the direct fabrication of complex metallic components [10]. In biomedical applications, the technology provides an ability to print implants to the exact size and geometry optimized for individual patients, revolutionizing their effectiveness [11]. While producing near-net shape components is ideal for

manufacturing complex, low production parts, the technology greatly restricts, if not eliminates, the ability to cold work materials after printing. It was well established in the 1980's that precipitation strengthening alone in binary NiTi alloys does not result in high enough yield stresses to promote stable superelastic performance for thousands to millions of cycles [2,5,7,9]. Given the current state of the art in developing shape memory alloys to achieve high strength through precipitation hardening alone, NiTiHf alloys have been identified as some of the best candidates to pursue [12–14].

NiTiHf alloys have primarily been proposed for use in high-temperature aerospace and automotive actuation applications where NiTi cannot perform (>100 °C), as Hf additions elevate the transformation temperatures [13,14]. Hence, most research to date has focused on the shape memory and superelastic behavior of NiTiHf alloys with a high Hf content (15–30 at.%). For these materials, strength and shape memory behaviors are strongly influenced by H-phase nano-precipitates [12–16]. Han et al. first reported the existence of H-phase precipitates in NiTiHf alloys [17], and recently Yang et al. [18] proposed a complete atomic structural model for H-phase.

Aging is an effective way to increase the matrix strength in these alloys by forming fine precipitates that act as pinning sites against the movement of dislocations, while still allowing the martensitic transformation to occur nearly unimpeded. These studies show that in slightly Ni-rich compositions, aging at 550 °C for 3 h is the preferred heat

treatment to achieve high recoverable strain, high strength, excellent superelastic behavior, and microstructural and dimensional stability due to presence of a homogeneous distribution of densely packed nanosized precipitates throughout the matrix [19–23].

It is already reported that H-phase precipitates are richer in Ni and Hf, their homogeneous distribution in the high (>15 at.%) Hf containing alloys can be attributed to Hf supersaturation in materials that are only slightly Ni-rich, such as the widely studied $Ni_{50.3}(Ti,Hf)_{49.7}$ type alloys. However, alloys with lower Hf content in this stoichiometry range have not been as widely investigated and the effects of heat treatments on H-phase precipitation and resulting properties in these compositions are not currently understood.

This study is part of a larger effort to develop new NiTiHf alloys that can be produced by additive manufacturing for biomedical implants. Consequently, the alloys have to be (mostly) austenitic at body temperature (austenite finish temperature $A_f < 37$ °C in most cases) and thus lower Hf content (6–9 at.%) materials were investigated. In order to strengthen the alloys solely through H-phase precipitation hardening, initially, we tried the same heat treatments found to be close to optimal in the more Hf-rich compositions (Hf > 15 at.%), a single step 550 °C for 3 h aging treatment. However, we found that this treatment did not sufficiently strengthen the alloys. Thus, we looked to recent reports that low temperature thermal cycling combined with room temperature aging leads to Ni clusters that are precursors to the formation of Ni_4Ti_3 precipitates in binary NiTi alloys [24], and hypothesized that analogous low temperature diffusion may result in improved H-phase precipitate morphologies in these moderate Hf-content NiTiHf alloys. In testing the hypothesis, we found that a two-step aging treatment comprised of 1) a low-temperature pre-aging heat treatment, followed by 2) the aging treatment established for higher Hf content alloys, to be effective for these moderate Hf compositions. Hence, we proceeded to investigate the effects and mechanisms of this 2-step treatment on NiTiHf alloys with moderate Hf content.

NiTiHf alloys with target compositions of $Ni_{50.3}Ti_{50-x}Hf_x$, with x = 6, 8, 8.5, and 9 at.% were made by induction-melting high-purity elemental constituents using a graphite crucible and casting into a copper mold. The ingots were homogenized in vacuum at 1050 °C for 72 h and then extruded at 900 °C at a 7:1 area reduction ratio. The extruded rods were sectioned into samples that were initially solution-annealed at 1050 °C for 30 min, water quenched, and then pre-aged at 300 °C for 12 h and air-cooled, and finally aged a second time at 550 °C for 3.5 h and air-cooled. To isolate the effect of pre-aging on the functional properties of NiTiHf alloys, other test samples were directly aged at 550 °C for 3.5 h after the solution-anneal treatment (without pre-aging at 300 °C for 12 h).

Mechanical compression tests were performed on an MTS servo-hydraulic load-frame equipped with an MTS 661.20 load cell. Compression samples were cylindrical with a diameter of 5 mm and a length of 10 mm. Five compression cycles were applied to the samples using a maximum load of 40 kN and a minimum load of 250 N, corresponding to 2 GPa and 13 MPa engineering stress limits. A cross-head speed of 0.1 mm/min was used, corresponding to an approximate strain rate of $10^{-4}\,s^{-1}$ and Ncorr digital image correlation (DIC) software [25] was used to analyze the displacements of the sample. Before each test, eight images of the undeformed sample were acquired and analyzed to establish the strain noise for each pattern, which fell between 10^{-4} to 10^{-5} for the data reported in Fig. 1.

Conventional and high-resolution transmission electron microscopy (HRTEM) of aged NiTiHf samples was carried out using an FEI Talos TEM (FEG, 200 kV). The TEM foils were prepared by electropolishing at an electrolyte of 30% HNO_3 in methanol (by volume) at around −35 °C. To measure the size of H-phase precipitates and interparticle distance (the distance of a single precipitate from its closest precipitate), several HRTEM images taken from various regions, were used. This measurement was repeated for almost 100 precipitates on each sample and average precipitate size, average interparticle distance and their corresponding standard error is reported.

Fig. 1 shows the compression responses of the NiTiHf alloys aged at 550 °C for 3.5 h, with (a–d) and without (e–h) an initial pre-aging treatment of 300 °C for 12 h. These tests were performed at room temperature (23 °C), and all the samples were austenitic at the start of the test. They then formed stress-induced martensite upon loading. Depending on the heat treatment, some of the remnant strains when they samples were unloaded can be attributed to martensite that did not transform back to austenite. The amount of strain that was due to retained martensite was phenomenologically assessed by heating the samples to 150 °C and measuring the recovered strains, indicated by the solid arrows in the figure. Strain that was not recovered in this process is phenomenologically attributed to plastic deformation, though we note microscopically, the two mechanisms (retained martensite and plasticity) are usually coupled. Complete recovery of the strain (almost 4%) was observed for all the NiTiHf samples that were pre-aged at 300 °C for 12 h (solid arrows in Fig. 1a–d). For the other samples with 6 to 8.5 at.% Hf (Fig. 1e–f), only a portion of the strain was recovered upon
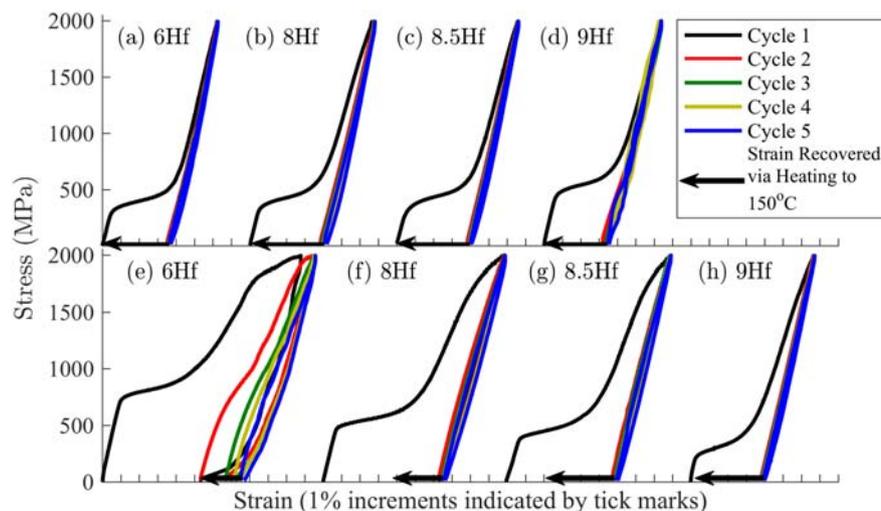

Fig. 1. Mechanical behavior of $Ni_{50.3}Ti_{42.7}Hf_6$, $Ni_{50.3}Ti_{41.7}Hf_8$, $Ni_{50.3}Ti_{41.2}Hf_{8.5}$, and $Ni_{50.3}Ti_{40.7}Hf_9$ (at. %) alloys in compression with (a–d) and without (e–h) the pre-aging treatment at 300 °C for 12 h followed by normal aging at 550 °C for 3.5 h for all samples.
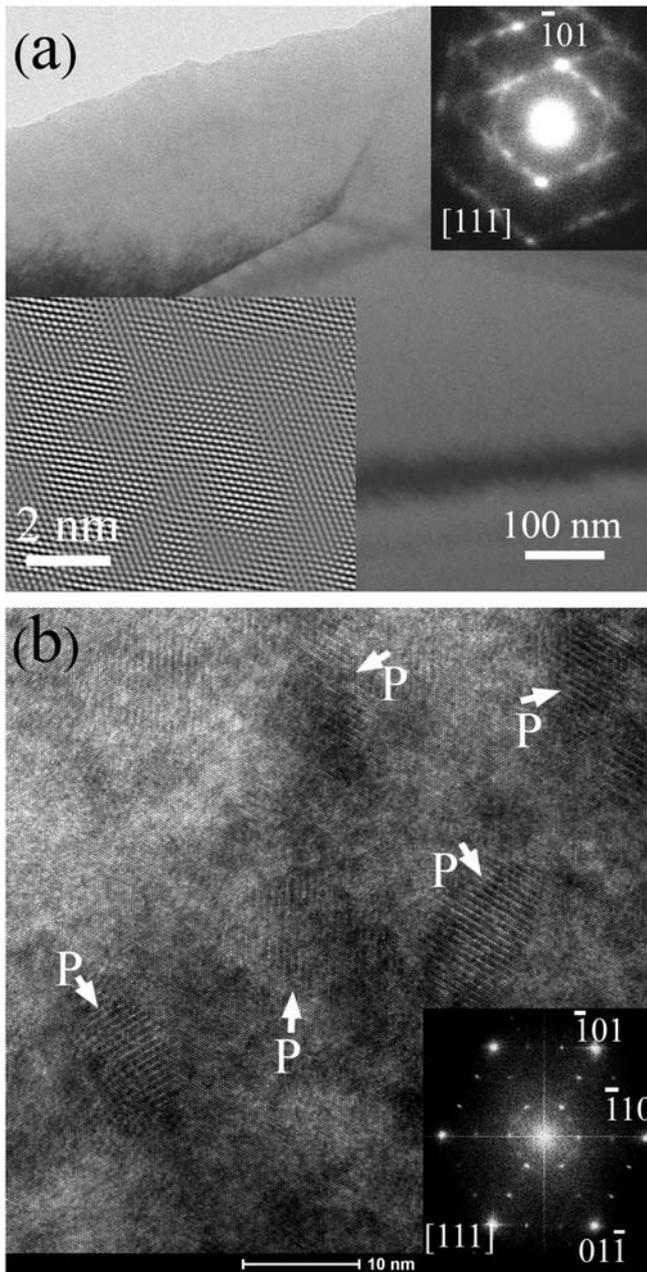
Fig. 2. (a) Conventional BF image of $Ni_{50.3}Ti_{41.2}Hf_{8.5}$ after pre-aging at 300 °C for 12 h. Corresponding SAED along [111] zone axis is shown in the lower left inset. (b) HRTEM micrograph along [111] zone axis of $Ni_{50.3}Ti_{41.2}Hf_{8.5}$ alloy pre-aged at 300 °C for 12 h and subsequently aged at 550 °C for 3.5 h.

heating, indicating a stronger presence of plasticity in the mechanical responses sans pre-aging. For the $Ni_{50.3}Ti_{40.7}Hf_9$ sample (Fig. 1g), however, the strain was fully recovered sans pre-aging, as well as in the

pre-aged case. While we did not directly observe superelastic behavior in this study, these data do suggest that the pre-aged samples and the un-pre-aged 9Hf sample would likely exhibit stable superelastic responses at higher test temperatures.

Fig. 2a shows a representative bright field (BF) TEM image of the $Ni_{50.3}Ti_{41.2}Hf_{8.5}$ sample after pre-aging at 300 °C for 12 h. Fully formed H-phase precipitates were not observed. The corresponding selected area electron diffraction pattern (SAED) of the $[111]_{B2}$ zone (upper right inset in Fig. 2a) confirms this observation, as the characteristic super-reflection of H-phase precipitates along ⟨110⟩ directions were not detected; however, a clear structured pattern of diffuse intensity is present. This pattern of diffuse intensity was also observed for other samples with different Hf content after pre-aging at 300 °C for 12 h. A filtered HRTEM study of the sample further corroborated the lack of fully formed H-phase precipitates after pre-aging at 300 °C for 12 h (as demonstrated in the lower left inset in Fig. 2a). The observed local distortion in HRTEM image may be due to existence of local strain field originated from Ni and/or Hf clustering during pre-aging.

These diffuse intensities with periodical character in reciprocal space indicate the existence of short-range order in the real-space lattice. Such diffuse intensities have been reported in binary $Ni_{50.6}Ti_{49.4}$ after low-temperature aging and were attributed to the existence of microdomains in the form of clusters of Ni atoms as precursors to full formation of Ni_4Ti_3 nanoprecipitates [24]. Analysis of H-phase precipitates in NiTiHf alloys indicates that the Hf content of the H-phase is higher than the Hf content in the matrix while the Ni content is also slightly higher in the precipitate compared with the matrix [19]. It is therefore expected that Hf and/or Ni atom clusters form after low-temperature aging (pre-aging treatment) as a precursor to H-phase precipitation upon further aging at higher temperatures, similar to the sequence of mechanisms that give rise to Ni_4Ti_3 nano-precipitation in binary NiTi alloys.

Fig. 2b is a HRTEM micrograph of the $Ni_{50.3}Ti_{41.2}Hf_{8.5}$ alloy pre-aged at 300 °C for 12 h and subsequently aged at 550 °C for 3.5 h. The corresponding fast Fourier transform (FFT) is shown in the upper left inset. The primary spots in the FFT result from the B2 cubic austenite structure, and the super reflections at 1/3 positions along ⟨110⟩$_{B2}$, are reflections from uniquely oriented H-phase precipitates (shown by the letter "P"). The H-phase precipitate dimensions for the different alloy compositions and heat treatments are presented in Table 1. For all the pre-aged samples, regardless of Hf content, the H-phase precipitates nucleated homogenously inside the grains and heterogeneous precipitation on GBs was not observed. The precipitates were ellipsoidal in shape with average dimensions of 14 ± 1 nm (length) and 7 ± 1 nm (width); the interparticle distance was 8 ± 1 nm. Variations in H-phase precipitate morphologies were not detectable for any of the pre-aged NiTiHf alloys using these TEM-based techniques; hence changes in their volume fractions are also unexpected. Therefore, the fully reversible 4% deformation depicted in Fig. 1a–d is aided by the uniform distribution of finely spaced H-phase precipitates, which strengthen the matrix against plastic deformation, while not impeding the formation of martensite.

The microstructure of the $Ni_{50.3}Ti_{42.7}Hf_6$ alloy that was aged at 550 °C for 3.5 h (without pre-aging) is shown in the BF-TEM micrographs of Fig. 3a and b taken from the vicinity of a GB and the interior of the

Table 1
H-phase precipitate dimensions for $Ni_{50.3}Ti_{49.7-x}Hf_x$ alloys (x = 6, 8, 8.5, 9 at.%) with and without pre-aging at 300 °C for 12 h followed by normal aging at 550 °C for 3.5 h. For the latter case (without pre-aging), characteristic precipitate morphologies are described for both regions at grain boundaries (GB) as well as within the grain interiors.

	With pre-aging	Without pre-aging				
	All alloys	$Ni_{50.3}Ti_{42.7}Hf_6$ (GB)	$Ni_{50.3}Ti_{42.7}Hf_6$ (interior grain)	$Ni_{50.3}Ti_{41.2}Hf_{8.5}$ (GB)	$Ni_{50.3}Ti_{41.2}Hf_{8.5}$ (interior grain)	$Ni_{50.3}Ti_{40.7}Hf_9$ (GB & interior)
Length (nm)	14 ± 1	60 ± 4	110 ± 10	43 ± 1	93 ± 2	23 ± 1
Width (nm)	7 ± 1	15 ± 2	57 ± 5	12 ± 1	25 ± 1	10 ± 1
Interparticle distance (nm)	8 ± 1	5 ± 1	95–700	5 ± 1	100 ± 4	12 ± 1
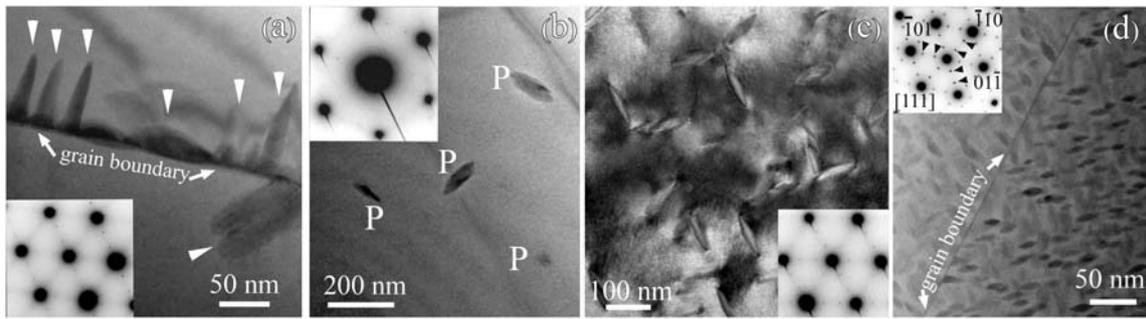
Fig. 3. Conventional BF images of (a, b) $Ni_{50.3}Ti_{42.7}Hf_6$, (c) $Ni_{50.3}Ti_{41.2}Hf_{8.5}$, and (d) $Ni_{50.3}Ti_{40.7}Hf_9$ after aging at 550 °C for 3.5 h without the pre-aging treatment. All corresponding SAED patterns shown in each insets are along the [111] zone axis of the B2 structure. The fundamental reflections are indexed at the inset of Fig. 3d and the super reflections originated from H-phase precipitates are marked with arrowheads.

austenite grain, respectively. It is apparent that aging of the $Ni_{50.3}Ti_{42.7}Hf_6$ alloy at 550 °C for 3.5 h induces heterogeneous nucleation of spindle-like H-phase precipitates along GBs (with an aspect ratio of 4) and a sparse distribution of larger, longer, and widely spaced ellipsoidal H-phase precipitates (with an aspect ratio of 2) in the interior of the grains, though the major part of the grain shown in Fig. 3b is actually free of precipitates. GBs are well known locations for heterogeneous nucleation in solid state precipitation processes because they decrease the interfacial energy between the precipitate and the parent phase, reduce stress fields, and because of the chemical composition gradient that exists around GBs [26]. However, because there is competitive growth on the GBs, the size of the grain boundary precipitates is small compared with the precipitates formed in the grain interiors.

With an increase in Hf content, the interparticle distance and size of the precipitates formed on the GB's and inside the grains decreases, as shown in Fig. 3c for the $Ni_{50.3}Ti_{41.2}Hf_{8.5}$ sample (Table 1). This suggests that there is transition from heterogeneous precipitation in the 550 °C aged NiTiHf alloys (for low Hf content) to homogeneous precipitation in alloys with higher Hf content for the same Ni:(Ti + Hf) ratio. The microstructure of $Ni_{50.3}Ti_{40.7}Hf_9$ after aging at 550 °C for 3.5 h (without pre-aging) is shown in Fig. 3d. Clearly, the H-phase precipitates are homogenously nucleated and distributed in grain interiors and regions near GBs; heterogeneous GB precipitation is not observed. Consistent with the microstructural observations, the amount of permanent strain observed during compression testing decreased as the Hf content increased from 5.7% (Fig. 1e for $Ni_{50.3}Ti_{42.7}Hf_6$) to 2% (Fig. 1g for $Ni_{50.3}Ti_{41.2}Hf_{8.5}$), and finally, full recovery without permanent deformation was observed for the $Ni_{50.3}Ti_{40.7}Hf_9$ alloy, where precipitation was homogeneous and finely spaced.

Finally, we note that the stresses required to form martensite (the plateau stresses) for the samples that were pre-aged at 300 °C for 12 h were relatively consistent, falling between 410 and 510 MPa (Fig. 1a–d), yet in contrast, the martensite formation plateau stresses for the samples without the pre-aging treatment (Fig. 1e–h) continuously decreased from 810 MPa to 300 MPa as Hf content increased from 6 to 9 at.%. In the former case, we hypothesize that the previously discussed chemical diffusion mechanism that is promoted by pre-aging also promotes more available hafnium to go into H-phase precipitates as the overall Hf-content is increased for each different composition. Contrarily, the changes observed in the plateau stresses in the latter case (no pre-aging) are logically expected from the increase in overall Hf content of each alloy, given that for most of the compositions, H-phase precipitation is not uniform enough throughout the matrix to effect the transformation temperatures greatly. Increasing the Hf content in NiTiHf alloys increases the Martensite start (M_s) temperature [27], thus through the Clausius-Clapeyron relation, the martensite formation stresses would decrease given a constant test temperature [28].

In summary, pre-aging $Ni_{50.3}Ti_{49.7-x}Hf_x$ alloys (x = 6, 8, 8.5, 9 at.%) at 300 °C for 12 h after solution annealing at 1050 °C leads to a higher density of the H-phase precipitates during subsequent aging at 550 °C,

than aging alone. This results in greater strength and subsequently improved mechanical and functional performance with 4% recoverable compression strain. The results suggest that Hf or other atom clusters form during the pre-aging treatment resulting in nucleation of a uniform distribution of H-phase when subsequently aged at 550 °C. Aging NiTiHf alloys at 550 °C directly after the solution annealing treatment (without pre-aging), leads to heterogeneous nucleation of H-phase precipitates on the GBs in the lower Hf compositions (6 to 8 at.%). Most of the grain interior is free of the precipitates, which results in reduced strength and leads to poor mechanical behavior. However, as Hf content is increased, homogenous precipitation is achieved directly, without pre-aging. As a result, mechanical and functional behavior is improved compared to the compositions with lower Hf content and no pre-aging.

References

[1] C.M. Wayman, K. Otsuka, Shape Memory Materials, Cambridge University Press, Cambridge, 1999.
[2] K. Otsuka, X. Ren, Prog. Mater. Sci. 50 (2005) 511–678.
[3] S. Miyazaki, K. Otsuka, ISIJ Int. 29 (1989) 353–377.
[4] J. Beyer, J. Phys. IV 5 (1995) 433–442.
[5] T.W. Duerig, K.N. Melton, D. Stockel, C.M. Wayman, Engineering Aspects of Shape Memory Alloys, Butterworth-Heinemann, Boston, 1990.
[6] K. Gall, H.J. Maier, Acta Mater. 50 (2002) 4643–4657.
[7] D.A. Miller, D.C. Lagoudas, Mater. Sci. Eng. A 308 (2001) 161–175.
[8] J. Khalil-Allafi, B. Amin-Ahmadi, J. Mater. Sci. 45 (2010) 6440–6445.
[9] M.J. Drexel, G.S. Selvaduray, A.R. Pelton, Proc. Int. Conf. Shape Mem. Superelastic Technol. (2006) 447–454.
[10] M. Elahinia, N. Shayesteh, M. Taheri, A. Amerinatanzi, B.A. Bimber, R.F. Hamilton, Prog. Mater. Sci. 83 (2016) 630–663.
[11] M. Elahinia, N. Shayesteh Moghaddam, M. Taheri Andani, A. Amerinatanzi, B.A. Bimber, R.F. Hamilton, Prog. Mater. Sci. 83 (2016) 630–663.
[12] G.S. Bigelow, A. Garg, S.A. Padula, D.J. Gaydosh, R.D. Noebe, Scr. Mater. 64 (2011) 725–728.
[13] O. Benafan, R.D. Noebe, S.A. Padula, R. Vaidyanathan, Metall. Mater. Trans. A 43 (2012) 4539–4552.
[14] H.E. Karaca, E. Acar, H. Tobe, S.M. Saghaian, Mater. Sci. Technol. 13 (2014) 1530–1544.
[15] L. Patriarca, H. Sehitoglu, Scr. Mater. 101 (2015) 12–15.
[16] A. Evirgen, I. Karaman, R. Santamarta, J. Pons, R.D. Noebe, Acta Mater. 83 (2015) 48–60.
[17] X.D. Han, R. Wang, Z. Zhang, D.Z. Yang, Acta Mater. 46 (1998) 273–281.
[18] F. Yang, D.R. Coughlin, P.J. Phillips, L. Yang, A. Devaraj, R.D. Noebe, M.J. Mills, Acta Mater. 61 (2013) 3335–3346.
[19] D.R. Coughlin, P.J. Phillips, G.S. Bigelow, A. Garg, R.D. Noebe, M.J. Mills, Scr. Mater. 67 (2012) 112–115.
[20] H.E. Karaca, S.M. Saghaian, G. Ded, H. Tobe, B. Basaran, H.J. Maier, R.D. Noebe, Y.I. Chumlyakov, Acta Mater. 61 (2013) 7422–7431.

[21] S.M. Saghaian, H.E. Karaca, H. Tobe, A.S. Turabi, S. Saedi, S.E. Saghaian, Y.I. Chumlyakov, R.D. Noebe, Acta Mater. 134 (2017) 211–220.

[22] A. Evirgen, I. Karaman, R. Santamarta, J. Pons, C. Hayrettin, R.D. Noebe, Acta Mater. 121 (2016) 374–383.

[23] A. Evirgen, F. Basner, I. Karaman, R.D. Noebe, J. Pons, R. Santamarta, Funct. Mater. Lett. 5 (2012) 1250038.

[24] S. Pourbabak, X. Wang, D. Van Dyck, B. Verlinden, D. Schryvers, Funct. Mater. Lett. 10 (2017) 1740005–1740011.

[25] J. Blaber, B. Adair, A. Antoniou, Exp. Mech. 55 (2015) 1105–1122.

[26] J. Khalil-Allafi, A. Dlouhy, G. Eggeler, Acta Mater. 50 (2002) 4255–4274.

[27] R. Noebe, T. Biles, S. Padula, W. Soboyejo, T. Srivastan, Advanced Structural Materials: Properties, Design Optimization, and Applications', CRC Press, 2007 145.

[28] A.P. Stebner, G.S. Bigelow, J. Yang, D.P. Shukla, S.M. Saghaian, R. Rogers, A. Garg, H.E. Karaca, Y. Chumlyakov, K. Bhattacharya, R.D. Noebe, Acta Mater. 76 (2014) 40–53.